Current Biology 23, 2121–2129, November 4, 2013 ©2013 Elsevier Ltd All rights reserved http://dx.doi.org/10.1016/j.cub.2013.09.013

Article

Distinct Roles of the Cortical Layers of Area V1 in Figure-Ground Segregation

Matthew W. Self,[1,*] Timo van Kerkoerle,[1] Hans Supèr,[2,3,4] and Pieter R. Roelfsema[1,5,6]

[1]Department of Vision & Cognition, Netherlands Institute for Neuroscience, Meibergdreef 47, 1105 BA, Amsterdam, the Netherlands

[2]Department of Basic Psychology, University of Barcelona, Passeig Vall d'Hebron 171, 08035 Barcelona, Spain

[3]Institute for Brain, Cognition and Behavior (IR3C), Passeig Vall d'Hebron 171, 08035 Barcelona, Spain

[4]Catalan Institution for Research and Advanced Studies (ICREA), Passeig Vall d'Hebron 171, 08035 Barcelona, Spain

[5]Department of Integrative Neurophysiology, Center for Neurogenomics and Cognitive Research, VU University, De Boelelaan 1085, 1081 HV Amsterdam, the Netherlands

[6]Psychiatry Department, Academic Medical Center, Postbus 22660, 1100 DD Amsterdam, the Netherlands

Summary

Background: What roles do the different cortical layers play in visual processing? We recorded simultaneously from all layers of the primary visual cortex while monkeys performed a figure-ground segregation task. This task can be divided into different subprocesses that are thought to engage feedforward, horizontal, and feedback processes at different time points. These different connection types have different patterns of laminar terminations in V1 and can therefore be distinguished with laminar recordings.

Results: We found that the visual response started 40 ms after stimulus presentation in layers 4 and 6, which are targets of feedforward connections from the lateral geniculate nucleus and distribute activity to the other layers. Boundary detection started shortly after the visual response. In this phase, boundaries of the figure induced synaptic currents and stronger neuronal responses in upper layer 4 and the superficial layers ~70 ms after stimulus onset, consistent with the hypothesis that they are detected by horizontal connections. In the next phase, ~30 ms later, synaptic inputs arrived in layers 1, 2, and 5 that receive feedback from higher visual areas, which caused the filling in of the representation of the entire figure with enhanced neuronal activity.

Conclusions: The present results reveal unique contributions of the different cortical layers to the formation of a visual percept. This new blueprint of laminar processing may generalize to other tasks and to other areas of the cerebral cortex, where the layers are likely to have roles similar to those in area V1.

Introduction

Neocortex is often divided into six layers on the basis of histological data. Every layer receives a characteristic pattern of inputs and gives rise to a distinct set of projections to other layers and brain structures. While the anatomy of the different layers is fairly well defined [1–4], the roles of the different layers in cortical processing are still poorly understood, and their elucidation remains a central challenge for systems neuroscience [5]. In the present study, we examined the role of the layers in the primary visual cortex (V1) of monkeys. V1 receives feedforward connections from the lateral geniculate nucleus (LGN) that terminate primarily in layers 4 and 6 [6, 7]; there are horizontal connections between the V1 columns that are present in all layers but predominantly terminate in upper layer 4 and the superficial layers [8, 9], and there are feedback connections from higher visual areas, which terminate primarily in layers 1 and 5 and tend to avoid layer 4 [9–12]. What is the role of these different inputs? Do they give rise to distinct types of firing behavior in the different layers?

To determine the role of the layers, we used a texture-segmentation task (Figure 1A), because electrophysiological [13], psychophysical [14, 15], and computational [16–18] studies have suggested that cortical processing in this task consists of a number of processing phases for which feedforward, horizontal, and feedback connections play different roles. First, the orientation of the line elements is extracted by the spatial arrangement of feedforward connections from the LGN to V1 [19]. Then, the edges between figure and background are detected at locations where the orientation changes abruptly (Figure 1B). This is thought to be achieved through horizontal inhibition between neurons with nearby receptive fields (RFs) tuned to the same orientation [16, 17, 20, 21], suppressing neuronal responses to homogeneous image regions. Finally, all image elements of the figure must be grouped together in perception (Figure 1C). Electrophysiological studies have shown that neuronal responses evoked by the figure are enhanced relative to the background, an effect known as figure-ground modulation (FGM) [22]. FGM in the figure center is thought to arise from feedback projections from higher visual areas back to V1, as it is modulated by attention [18] and is absent when a monkey fails to detect the figure [23] or is anesthetized [24].

The aim of our study was to identify the laminar circuits engaged by the different processing phases in the texture-segregation task of Figure 1A. We simultaneously recorded multiunit neural activity (MUA) from all layers of V1 using a multicontact depth electrode. The advantage of this electrode is that we were also able to measure the flow of synaptic currents in the different layers underlying changes in firing rate using current-source density (CSD) analysis [25]. The laminar profile of these currents can be compared to the targets of feedforward, horizontal, and feedback connections, allowing us to estimate the contributions of these connection types to figure-ground segregation.

Results

We trained two monkeys to perform a texture-segregation task (Figures 1D and 1E) where they saw a square figure of one orientation on a background of the opposite orientation. Both monkeys performed this task with an accuracy of greater than 95%.

Twenty-five percent of trials were catch trials without a figure, and on these trials, the monkey was rewarded for maintaining fixation. The performance on catch trials was slightly

*Correspondence: m.self@nin.knaw.nl

CrossMark

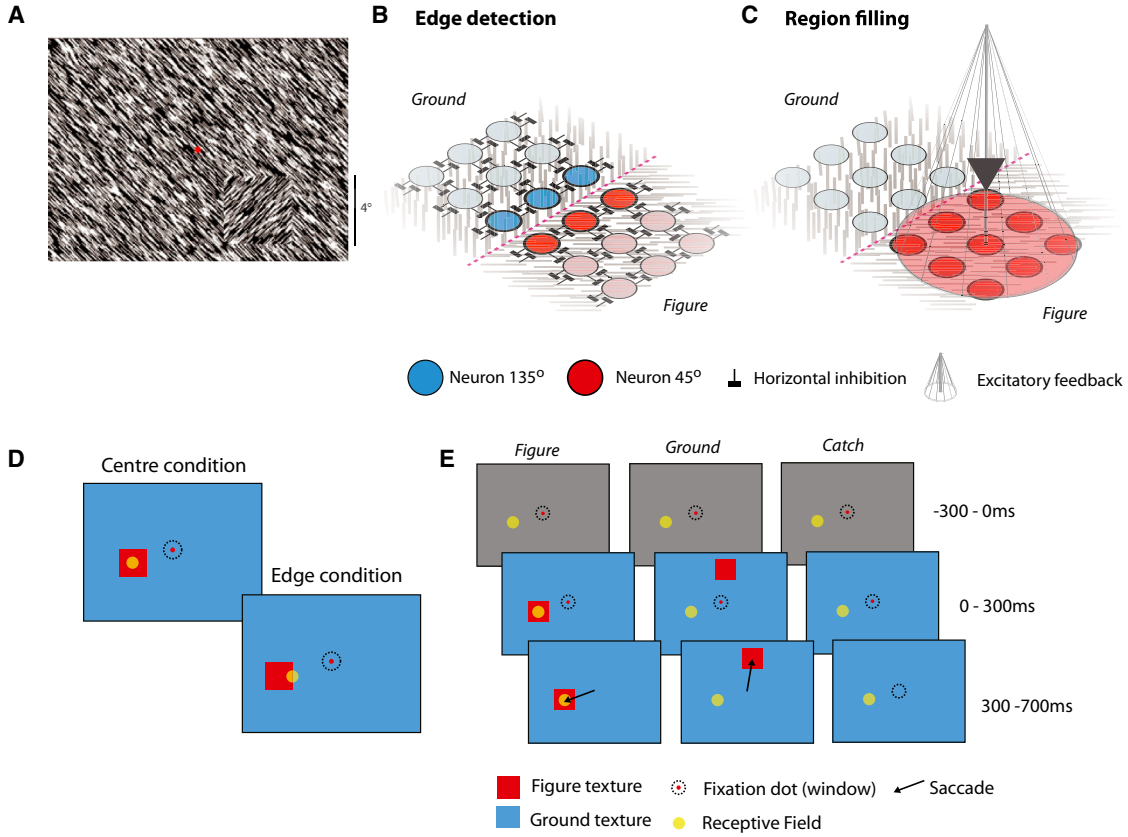

Figure 1. Stimulus and Task Design

(A) Example texture with an orientation-defined figure used in the present study.

(B) A model of neural responses at either side of a texture boundary (pink dashed line). Neurons tuned to the same orientation inhibit each other (black bars). A neuron at the edge of the figure receives less inhibition than a neuron in the middle of the texture and therefore has a relatively enhanced firing rate (saturated colors, thicker outlines).

(C) Models of region filling suggest that the figure region becomes perceptually grouped through excitatory feedback from neurons in higher visual areas tuned to the figural orientation (red cone), causing an enhanced firing rate in the entire figure region.

(D) We varied the eccentricity of the figure in blocks of 200–500 trials so that the receptive field (RF) of the neurons fell on either the figure center or edge.

(E) Schematic representation of the time course of the task. Monkeys started a trial by fixating within a small window (1°) centered on a fixation point. After 300 ms, a figure-ground texture appeared. There were three possible figure locations. One was centered on the neurons' RF (figure condition), and the other two were at an angle of 120° (ground conditions). The orientation of the line elements (45° or 135°) was chosen so that the texture inside the RFs was on average the same across conditions. The fixation dot was extinguished after another 300 ms, and the monkeys were rewarded for an eye movement to the figure (arrow). On catch trials there was no figure, and the monkey was rewarded for maintaining fixation. The yellow circle denotes the RF, and the red square illustrates the location of the figure.

lower (77% for monkey S and 89% for monkey E) due to the longer fixation time.

Visually Driven Activity in the Different Cortical Laminae

We recorded MUA simultaneously from the different laminae of area V1 using a multicontact electrode (Figure 2A). We estimated the cortical layer of each electrode site using CSD analysis (see Experimental Procedures and Figures S1A–S1C available online). The CSD profile provides a reliable measure for the boundary between layers 4c and 5. We estimated boundaries between the other layers using data from previous anatomical studies [3, 4, 26], and these boundaries are therefore more tentative. For each electrode contact, we measured the orientation tuning and the multiunit RF with a moving bar stimulus (Figures S1D and S1E; Supplemental Experimental Procedures). We then examined the neural responses induced by the appearance of the textures in the catch trial condition, in which there is no figure-ground organization. Visual response latency (calculated using a curve-fitting technique; Figures 2B and 2C and Supplemental Experimental Procedures) varied across the cortical layers, being earliest in layer 4c and layer 6. Visually driven activity then spread to layer 5 and considerably later (10–15 ms) to the superficial layers. For statistical analysis, we grouped the layers into four laminar compartments (deep layers, layer 4c, layer 4a/b, and superficial layers; see Experimental Procedures). The differences in latency across the compartments were highly significant (assessed by a mixed linear model that corrects for the correlations within penetrations; see Supplemental Experimental Procedures for details; $F_{3,119.7} = 116$, $p < 0.001$, $n = 43$ penetrations). Post hoc tests showed that layer 4c had a significantly shorter latency and that the superficial layers had a significantly longer latency than all other compartments (all $p < 0.05$; Bonferroni corrections were applied to all post hoc tests).

Figure 2D shows the MUA response induced by the appearance of the texture averaged across all penetrations. Figure 2E shows the MUA and CSD responses during the initial peak response phase (30–90 ms). The CSD profile gives information

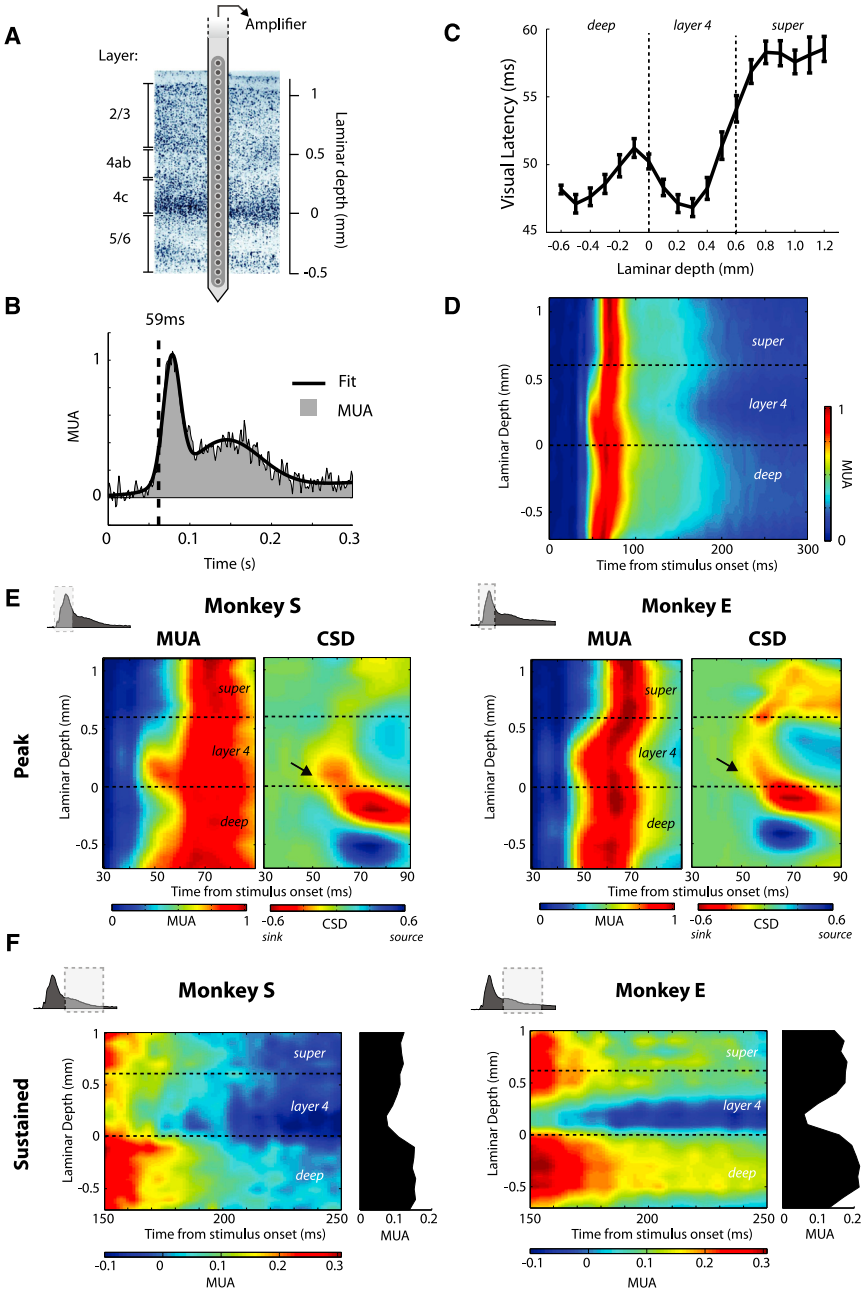

Figure 2. Visually Driven Activity across the Layers of V1

(A) Laminar electrode for the simultaneous recording of multiunit neural activity (MUA) and current-source density (CSD) at different cortical depths. The electrode ("U probe," Plexon) contained 24 contact points spaced 100 μm apart, which allowed us to record simultaneously from every layer of cortex. The diagram shows the approximate thickness of V1 cortex and the division into four layer compartments: 2/3, 4ab, 4c, and 5/6. We assigned the depth of 0 mm to the reversal in the CSD, which marks the boundary between layer 4c and layer 5.

(B) Example MUA response in the catch-trial condition (averaged across 235 trials) at one of the recording sites. A curve was fitted to estimate the visual response latency as the point at which it reached 33% of its maximum (dashed line).

(C) The black curve shows visual latencies in the different laminae, averaged across all penetrations, the error bars indicate SEM (Figure S5 specifies number of recording sites per cortical depth).

(D) The average MUA response across penetrations (n = 43) to the oriented texture (catch-trial condition). Dashed lines mark the boundaries between layer compartments.

(E) The average MUA and current-source density (CSD) responses evoked by the onset of the oriented texture across the different laminae in an early time window (30–90 ms). These responses were averaged across 29 penetrations for monkey S and 14 for monkey E. For the CSD plots on the right, warmer colors indicate current sinks (i.e., current flowing into neurons) and cooler colors indicate current sources (current flowing out of neurons). The first MUA response occurred in layers 4c and 6, and it was accompanied by a current sink in layer 4 (indicated by the black arrows).

(F) MUA during the more sustained phase of the response (150–250 ms). The plots to the right of each graph show the average MUA in this time period for each layer. Note the U-shaped profile indicating that responses in layer 4 are more transient than in the superficial and deep layers.

See also Figure S1.

about the currents that flow in the cortical layers [25]. Current sinks mark the locations where excitatory input arrives and causes inward currents, whereas current sources arise at locations where the current flows out of cells. The first current in the average CSD was a sink in layer 4c reflecting the thalamic input into this layer (black arrow in Figure 2E). This sink coincided with a source in layer 5, which reflects the passive return of current [25]. This initial sink/source pair was followed by a pattern of current sinks and sources in superficial and deep layers that reflects the anatomy of the cortical microcircuitry [1]. Thus, the laminar recordings reveal how the visual response activates successive layers of V1.

The initial burst of activity evoked by the onset of the texture stimulus was followed by a period of sustained spiking activity (Figure 2F). We measured the strength of the sustained activity as the average MUA in a window from 100–300 ms after stimulus onset. The strength of this sustained response differed significantly between the cortical compartments (mixed model, $F_{3,119.8} = 9.9$, $p < 0.001$, n = 43 penetrations). Spiking activity in layer 4 was relatively transient, whereas the response was more sustained in the superficial layers and particularly in layer 5.

The Laminar Profile of Region Filling in V1

To examine the differences between neural responses evoked by the center of the figure and the background, we placed the figure so that the RF fell on its center or on the background. Figure 3 shows an example penetration from each monkey and illustrates several effects that we consistently observed across penetrations. The laminar profiles of the responses evoked by the figure and background were similar during the initial peak response, but at later time points (>100 ms), responses were stronger when the figure fell on the RF (Figures 3A and 3B). This can be best visualized by subtracting the background response from the figure response to compute

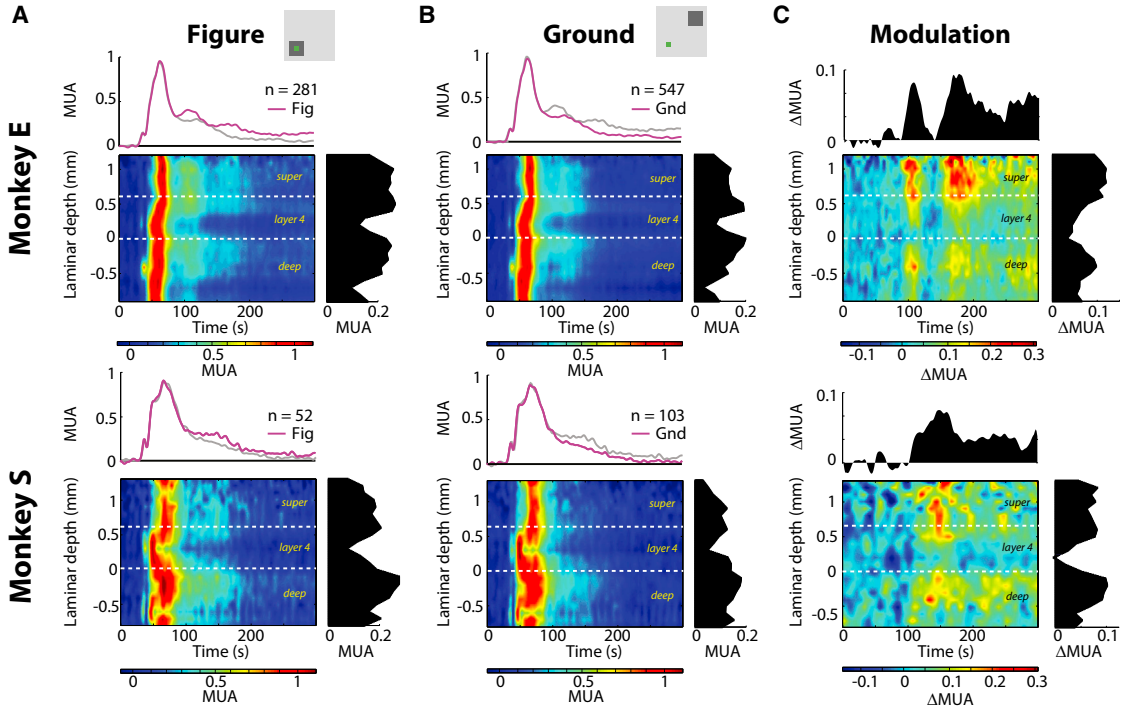

Figure 3. Laminar Differences in FGM in Two Example Penetrations

(A and B) MUA responses across the layers from an example penetration in monkey E (top graphs) and monkey S (bottom graphs) evoked by the figure (A) and background (B). The panels above show the MUA-response averaged across all laminae; the relevant condition is highlighted in pink. Panels to the right show the MUA response averaged across time (0–300 ms post stimulus onset). Note that the high levels of sustained activity in the superficial layers and in layer 5 are most pronounced in the figure condition. n, number of trials.

(C) Figure-ground modulation (FGM), which is the difference between activity evoked by a figure and the background. The upper graphs show how FGM develops in time, and the right graph shows the variation across laminae. Note that FGM is weakest in layer 4.

FGM (Figure 3C). In both example penetrations, FGM was strongest in the superficial and deep layers and considerably weaker in layer 4. The laminar pattern of FGM resembled the pattern of sustained activity (compare Figure 3C and Figure 2F). The strength of FGM differed significantly between laminar compartments of V1 in both example penetrations (two-way ANOVA, interaction between condition and compartment, monkey S: n = 155 trials, $F_{3,612} = 3.3$, $p = 0.02$; monkey E: n = 828 trials, $F_{3,3304} = 12.2$, $p < 0.001$).

We observed a similar laminar profile of FGM at the population level (Figure 4A). We quantified center FGM as the difference in normalized activity evoked by the figure and background (in a window from 100–300 ms). In monkey E, the average FGM was 0.072, i.e., the difference in response evoked by figure and ground was on average 7.2% of the peak response (mixed model, $F_{1,13.1} = 382$, $p < 0.001$, n = 14 penetrations). FGM was significant ($p < 0.05$, two-sample t test) at 98% of individual recording sites. In monkey S, the average FGM was 5.8% (mixed model, $F_{1,27.5} = 88.8$, $p < 0.001$, n = 29 penetrations) and was significant at 68% of sites. We did not observe cases where the background evoked significantly stronger activity than the figure. The absolute FGM strength may appear small, but this is due to the normalization to the peak response. During the sustained response period (100–300 ms), the figure-evoked responses were 46% (monkey E) and 28% (monkey S) stronger than the background. FGM was strongest in the superficial and deep layers, which are targets of feedback connections, and weaker in layer 4, the main target of feedforward input from the LGN (Figure 4A; data and statistical maps from the individual monkeys are shown in Figure S2). For statistical analysis, we again grouped the layers into four compartments (Figure 4C). FGM differed significantly between these compartments (mixed model, monkey S: $F_{3,78.0} = 5.4$, $p = 0.002$; monkey E: $F_{3,38.2} = 35.2$, $p < 0.001$). Post hoc analyses showed that the deep and superficial layers modulated significantly more than the layer 4 sites ($p < 0.05$) and were not significantly different from each other ($p > 0.5$). Control analyses showed that these results did not depend on the orientation tuning of the recording sites and were not caused by variations in eye position within the fixation window (Supplemental Results). Thus, FGM is strong in the superficial and deep layers, targets of feedback connections.

To examine the synaptic inputs responsible for FGM, we computed the difference between the CSD evoked by the figure and the background (Figure 5A). FGM was associated with an altered current flow in layer 5 and very superficially in putative layer 1 or upper layer 2 (black arrows in Figure 5A). There appears to be an additional current sink in the figure condition, but because Figure 5A is the result of a subtraction, it is also possible that there was an additional current source in the background condition (Figure S3A shows the figure and ground conditions separately). Cluster-based statistics indicated that the differences between the figure and background CSD described above were all statistically significant (Figure 5C; Supplemental Experimental Procedures). The latency of the CSD difference in layer 5 and layer 1/2 was approximately 100 ms, and it began at the same time as the

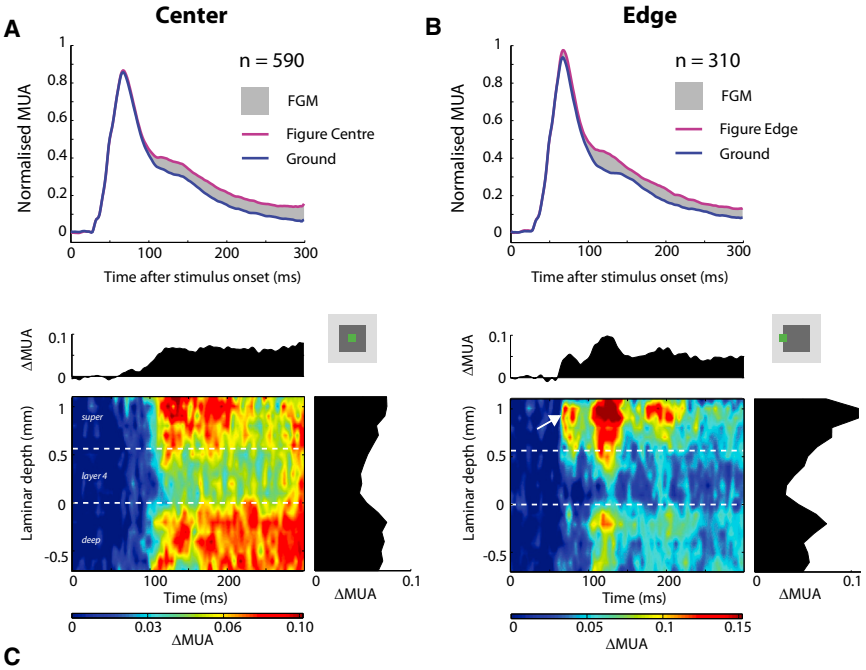

Figure 4. Laminar Differences in FGM across the Population of Recording Sites

(A and B) FGM in the center of the figure (A) and at the edge (B), averaged across all penetrations. The upper plots show MUA averaged across layers. The shaded gray region shows the difference in activity evoked by the figure and background (FGM). The lower plots show the laminar profile of FGM. The edge causes early FGM in the superficial layers (white arrow in B). n, number of recording sites.

(C) The average FGM evoked by the figure center in the four layer compartments. Error bars indicate SEM. Significant differences from post hoc tests in the average across both animals are indicated by the asterisks: *p < 0.05, **p < 0.01, ***p < 0.001 after Bonferroni correction.

(D) Difference between the level of FGM in the edge and center conditions during the early (50–100 ms) time period. Note that the difference is strongest in the superficial layers and, to a lesser extent, layer 4ab. Numbers of recording sites in (C) and (D) are specified in Figure S5.

See also Figure S2.

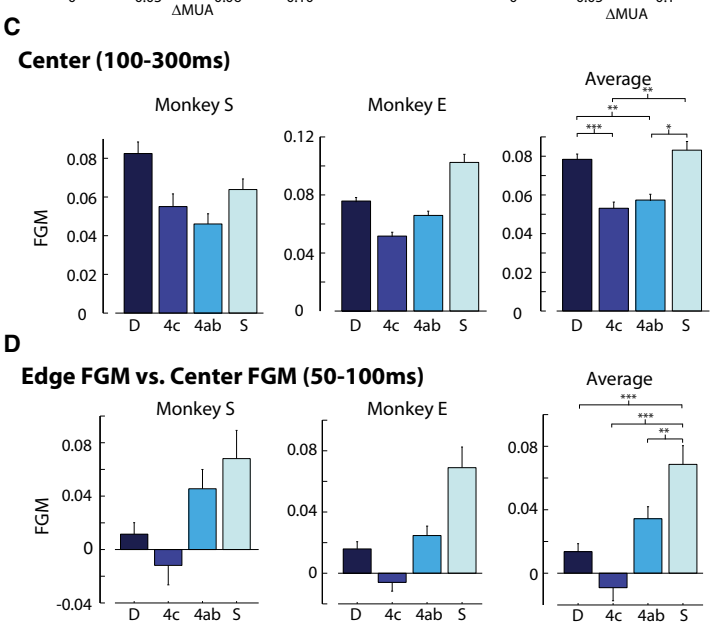

modulation of the MUA response (see below and Figure S4). Thus, our results indicate that region filling is caused by a putative excitatory input into layers 1, 2, and 5, the major targets of corticocortical feedback connections [10, 11].

Laminar Profile of FGM at Boundaries between Figure and Background

The boundary between figure and background was defined by an orientation discontinuity, which might be detected locally in V1. To examine the laminar profile of the boundary detection process, we placed the neurons' RF on the edge between figure and background (Figure 1D). We observed significant FGM at the figure edge for both monkeys (mixed model: monkey S: n = 16 penetrations, $F_{1,16.3} = 43.6$, $p < 0.001$; monkey E: n = 12 penetrations, $F_{1,11.2} = 197.3$, $p < 0.001$). At first sight, the laminar profile of edge FGM was similar to that of center FGM (Figures 4A and 4B; Figure S2). However, the edge of the figure evoked an additional, early increase in neuronal activity that was strong in the superficial layers (arrow in Figure 4B) and somewhat weaker but significant in upper layer 4 (Figures 4D and 6C). We tested almost all recording sites in the edge and the center condition so that we could compare the FGM for matched penetrations. FGM in an early analysis window (50–100 ms) was significantly stronger when the RF was on the edge of the figure than when it fell on the center (mixed model, n = 27 matched penetrations, $F_{1,26.6} = 6.3$, $p = 0.02$). This difference in FGM between the center and the edge varied between the laminar compartments ($F_{3,67.2} = 7.2$, $p < 0.001$), being significantly larger in the superficial layers than in the other layers (post hoc tests, all $p < 0.05$) (Figure 4D).

To further characterize edge FGM, we measured its latency using the same curve-fitting procedure used for the visual latency (Figures 6A and 6B). Across the population of recording sites, the early detection of edges in upper layer 4 and the superficial layers caused the latency of edge FGM to differ significantly between layers (mixed model, $F_{3,55.6} = 6.4$, $p = 0.001$). Edge FGM in the superficial layers began on average at 71 ms after stimulus onset (Figure 6C). In contrast, the latency of FGM in the center of the figure was very similar across the layer compartments (mixed model, $F < 1$) beginning at 100 ms. Center FGM was significantly later than edge FGM in the superficial layers and layer 4ab (paired t test, both $p < 0.005$). Edge FGM was accompanied by an extra current sink in putative upper layer 4/lower layer 3 (black arrow, Figures 5B and 5D) and a source in layer 2. Although these currents appear weak in Figure 5B, they were reproducible across penetrations and animals (Figures S3B and S3C) and occurred at a latency of 58 ms, just prior to the

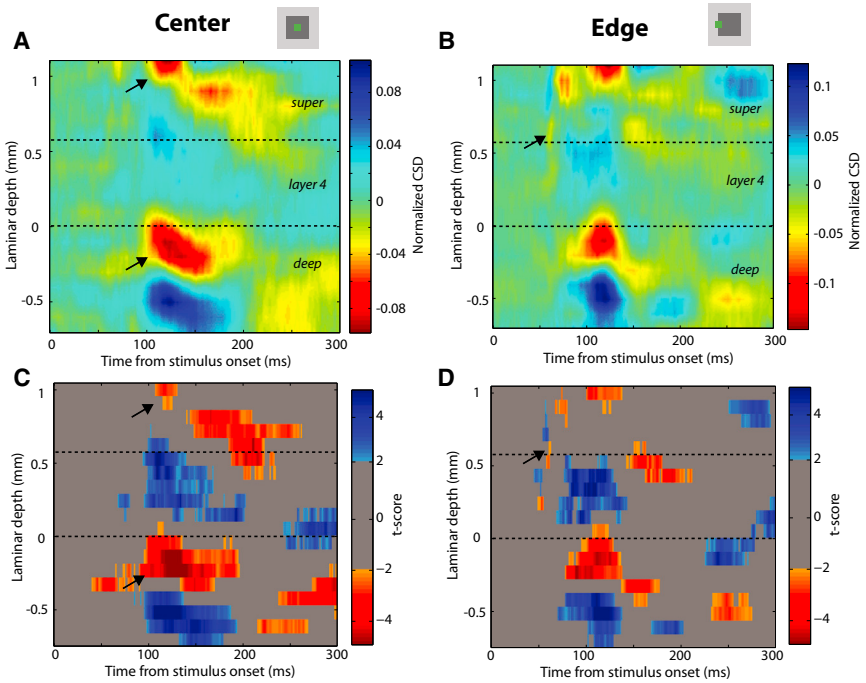

Figure 5. Differences in Current Flow between Figure and Background

(A) Difference in the normalized CSD evoked by the figure center and background. Warm colors show stronger sinks in the figure condition (and/or stronger sources in the ground condition), and cooler colors show stronger sources. The black arrows indicate the first sinks that differentiate between figure and background at a latency of ~100 ms in layer 5 and layer 1/2.

(B) The difference in CSD between the figure edge and the background. The earliest weak sink occurs in upper layer 4/superficial layers (black arrow). This sink was consistent across penetrations (see Figures S3B and S3C).

(C and D) A statistical map indicating the t score of the difference between the CSD evoked by the figure center (C) or figure edge (D) and the background. Cluster statistics were used to calculate the significance of sinks and sources. Nonsignificant clusters are not shown (gray area). Figure S5 specifies the number of recording sites per cortical depth.

See also Figure S3.

edge modulation of the MUA response (Figure S4), which suggests that they underlie the edge FGM. Thus, edge detection was associated with an early MUA increase in superficial layers and upper layer 4, caused by a characteristic pattern of synaptic input into these layers.

Discussion

Here we have examined the roles of the different cortical layers within a single visual task that requires a number of different computations. The segregation of a figure from the background starts with the registration of features, is followed by the detection of feature discontinuities at the figure boundaries, and completes with a region-filling process that labels all figural image elements with enhanced activity [13, 18]. We observed distinct contributions of the cortical layers to the successive processing phases, corresponding well to the anatomy of feedforward, horizontal, and feedback connections (summarized in Figure 7).

Flow of Visual Information through the Cortical Column

The initial input from the LGN into layer 4c causes large sinks in the CSD, and this input robustly drives responses in all cortical layers (Figure 7B). We observed that the latency of the visual response varies across the cortical laminae, in accordance with previous studies [27, 28]. The shortest latencies occurred in the input layers 4c and 6, with longer latencies in layer 5 and particularly in the superficial layers. This result is surprising, as the anatomy of the microcircuitry of V1 appears to predict shorter latencies in superficial layers than layer 5 [2, 29]. Long response latencies in the superficial layers have been observed previously [27], and their cause is unknown. One possibility is that neurons in the superficial layers must summate the input from layer 4 for a longer period before they reach spike threshold. Layer 5 neurons receive a small amount of direct input from layer 4 [30] onto their apical dendrites in layers 2/3 [31], which is highly effective in driving the neuron to threshold [32] and may allow layer 5 neurons to fire at a shorter latency. We also observed a laminar difference in the balance between transient and sustained activity. Layers 4 and 6 had a strong transient response, but their activity decreased after ~100 ms. Visually driven activity was more sustained in the superficial layers and layer 5 [33], and these layers may therefore play an important role in representing the stimulus at later times. These laminar differences contrast with a recent study in V1 of anesthetized monkeys [34], showing that the level of sustained activity evoked by moving gratings is relatively homogeneous across the layers. This discrepancy may have been caused by our use of stationary texture patterns, which cause stronger adaptation, or by a difference between the awake and anesthetized state.

Detection of Feature Discontinuities at Figure Edges

The figures used in this study were delimited by orientation-defined edges. Neurocomputational models have suggested that boundary detection is caused by inhibition between neurons tuned to the same orientation [20, 21]. This "iso-orientation inhibition" suppresses activity in image regions with a homogeneous orientation and is weaker at edges, thus accounting for edge FGM (Figure 1B) [35]. It has also been implicated in orientation pop-out detection in V1 [36, 37].

We observed early enhancements in spiking activity at orientation-defined edges within 10–15 ms after the visual response in the superficial layers and upper layer 4 (Figure 7C). This finding is in line with a recent study demonstrating that iso-orientation inhibition is most pronounced in these layers [38], and the latency is also in good agreement with previous studies [35, 36, 39]. Horizontal connections within V1 are a likely source of the required orientation-tuned inhibition. Many pyramidal neurons in V1 have axonal arbors that project horizontally over large distances [8, 40, 41] and are particularly prominent in upper layer 4 and the superficial layers [9], although these connections are also present in the other layers. These horizontal connections preferentially link cortical columns tuned to the same orientation, and they could therefore provide the required iso-orientation inhibition [42]. In

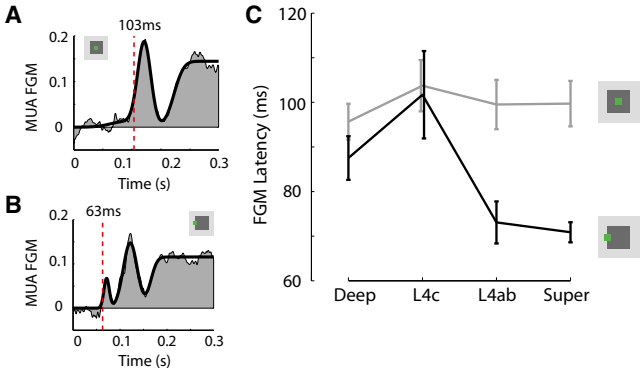

Figure 6. Analysis of the Latency of FGM

(A) Time course of FGM at an example recording site in the superficial layers, with RF in the center of the figure. The black line shows the function (the sum of two Gaussians and a cumulative Gaussian) used to estimate the latency of FGM (the same function was used to estimate visual latency). The latency was estimated as the time point at which the function reached 33% of its first maximum.

(B) Example FGM time course at a superficial layer electrode with the RF on the edge. Note that the first Gaussian captures the early edge modulation.

(C) The average latency across penetrations of the center FGM (gray line) and edge FGM (black line), calculated by fitting a curve to the FGM in each layer compartment for every penetration. Error bars show SEM. See Figure S5 for the number of recording sites per compartment.

See also Figure S4.

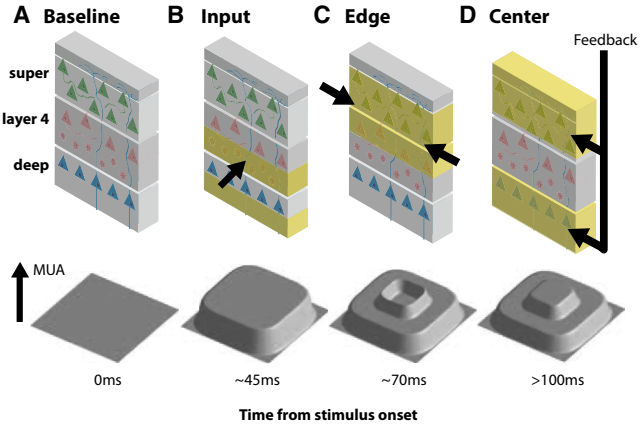

Figure 7. The Processes for Figure-Ground Segregation Have Different Time Courses and Specific Laminar Profiles within Area V1

The registration of features started in layers 4 and 6 (yellow region in B), the layers that receive input from the LGN, causing an early current sink in layer 4c (black arrow in B). Whereas the textures produced a transient response in layers 4 and 6, the response in the other layers was more sustained, especially in layers 2/3 and layer 5. After 65–70 ms, boundary detection occurred in the superficial layers (yellow regions in C) because image locations where the features changed caused stronger MUA activity than image locations with a homogeneous orientation. This edge enhancement was accompanied by current sinks in upper layer 4 and the superficial layers, which receive input from horizontally projecting axons within V1 (black arrows in C). After approximately 100 ms, FGM also occurred in the center of the figure (yellow region in D). Center FGM was significantly weaker in layer 4 than in the deep and superficial layers, and it coincided with additional current sinks in the upper superficial layers and in layer 5 (black arrows in D), known targets of corticocortical feedback connections.

accordance with a contribution of the horizontal connections, the earliest difference in current flow between the edge and center FGM was in upper layer 4 and the superficial layers (Figure 5B; Figures S3B and S3C) [8, 40]. An important role for local processing within V1 for boundary detection is also supported by a study demonstrating that blocking V2 did not reduce pop-out effects in V1 [43] and a recent study showing that boundary detection depends little on the animal's attentional state [18]. Our results, combined with these previous findings, support the idea that texture-defined boundaries are first detected locally in V1 through iso-orientation inhibition.

FGM at the Center of the Figure

Iso-orientation inhibition for boundary detection would cause suppression of neuronal activity in the center of the figure, where image elements are surrounded by the same orientation. We have previously postulated a complementary region-filling process where neurons in higher areas that register the figural orientation provide feedback to excite V1 neurons coding the same orientation [16, 44] (Figure 1C). This "iso-orientation excitation" feedback mechanism can explain why FGM in V1 labels all image elements of the figure with enhanced activity at a longer delay and is supported by a number of previous studies. FGM in V1 in the center of the figure is abolished if higher areas are lesioned [45] or if the monkey is anesthetized [24], and it is reduced if the animal directs attention away from the figure [18]. FGM in the figure center is also reduced if the monkey fails to detect the figure [23]. The present results provide further support for this view. Center FGM was strongest in the superficial and deep layers (Figure 7D), which receive feedback from higher areas, and it was weaker in the input layer 4 (Figures 4A and 4C). Moreover, the center FGM coincided with strong current sinks in layers 1, 2, and 5 (Figure 5A), which are prime targets of feedback connections to area V1 [9, 10, 46]. The areas that provide these feedback signals cannot be determined from our data, but the most likely candidates are V2 and ventral stream areas (e.g., V4), where neurons are selective for orientation and send feedback connections to the deep and superficial layers of V1 [9, 10, 12, 46]. The pattern of feedback targets we observe is less consistent with a contribution from dorsal stream areas such as MT that target layer 4B [47].

The influence of figure-ground organization on spiking activity was more widespread than the CSD sinks. We note, however, that these sinks may also reflect input into the dendrites of cells with somas located in different cortical layers. Furthermore, FGM can be passed around the cortical microcircuitry through the many interlaminar connections [1, 2]. Layer 4c neurons have only few dendrites extending into layers 1, 2, and 5 [2], which might cause them to receive little feedback from higher areas, and this could explain the weak FGM in this layer. However, it is also conceivable that the weaker FGM in layer 4 is the result of the weaker level of sustained activity. Previous studies suggested that feedback effects are particularly pronounced for neurons that are well driven by a stimulus and weaker for neurons that are not [48, 49]. Such a multiplicative interaction between feedback effects and visually driven activity could be conveyed by NMDA receptor-mediated feedback [50]. NMDA receptors only pass current if the membrane is depolarized, which could explain why FGM is strongest in layers with a high level of sustained activity.

In conclusion, the present results reveal distinct laminar patterns of neuronal activity in V1 for the visual response, the detection of boundaries, and the labeling of figural image regions with enhanced neuronal activity. Future studies can

now determine whether the laminar patterns observed in the present task comprise a canonical pattern for tasks that require feedforward activation, combined with local intra-areal processing and feedback from higher visual areas.

Experimental Procedures

All procedures complied with the NIH Guide for Care and Use of Laboratory Animals and were approved by the institutional animal care and use committee of the Royal Netherlands Academy of Arts and Sciences. We recorded from two adult macaque monkeys (monkeys S and E) using laminar electrodes (Figure 2A). The monkeys were implanted with a headpost and recording chamber as described previously [50]. We targeted the operculum of area V1 (visualized using ultrasonic imaging; Figure S1B) as well as the calcarine portion of V1 by inserting the electrode deeper into the cortex (Figure S1D).

We recorded the spiking responses of neurons as the envelope of the multiunit neural activity (MUA) (Supplemental Experimental Procedures). The local field potential was recorded by filtering the raw signal from the electrodes (digitized at 24.4 kHz), using a low-pass filter (second-order Butterworth filter, corner frequency 200 Hz), and sampling it at 763 Hz. The current-source density was calculated as

$$CSD(x) = -\sigma \cdot \frac{\varphi(x-h) - 2\varphi(x) + \varphi(x+h)}{h^2},$$

where φ is the voltage (in μV), x is the point at which the current-source density (CSD) is calculated, h is the spacing of recording sites for the computation (here, 200 μm), and σ is tissue conductivity (we used 0.4 S $\times$ m^{-1}).

The MUA response at each recording site was normalized by subtracting the spontaneous activity, measured from 150 to 0 ms before stimulus onset, and by dividing the response by the peak response (maximum in a 50–90 ms window after stimulus onset) in the catch-trial condition. Figure-ground modulation (FGM) was calculated as the difference between normalized figure and ground MUA responses in a time window from 100 to 300 ms after stimulus onset. We normalized the CSD of each penetration by dividing by the maximum absolute value of the CSD across layers during the peak period (50–90 ms) in the catch-trial condition.

To generate average MUAs and CSDs per electrode depth, we aligned the depth of the different penetrations using the CSD (Supplemental Experimental Procedures). The realigned, normalized CSD data and normalized MUA signals were then averaged across penetrations. We assigned recording sites to one of four laminar compartments based on their distance from the layer 4c/layer 5 boundary. The assignments were made with reference to previous anatomical studies [3, 4, 26] that measured the thickness of the cortical layers in V1. These assignments come with an inherent degree of uncertainty, as histological measurements of layer thicknesses vary between studies, aside from the CSD reversal at the boundary between layer 4 and layer 5 that is reliable [25]. The compartment labels we use in this paper should therefore be taken as guides and do not imply a one-to-one correspondence with histological data. Recording sites between 0.7 and 0.1 mm below the 4c/5 boundary were assigned to the deep layers, sites between 0 and 0.2 mm above the boundary were assigned to layer 4c, sites between 0.3 and 0.5 mm were assigned to upper layer 4 (which we refer to as layer 4ab), and sites more than 0.5 mm above the boundary were assigned to the superficial layers. Recording sites more than 0.7 mm below or more than 1.1 mm above the boundary were removed from the analysis because we did not obtain sufficient data from these very deep and very shallow locations (14.9% of all recording sites).

Supplemental Information

Supplemental Information includes five figures, Supplemental Data, and Supplemental Experimental Procedures and can be found online at http://dx.doi.org/10.1016/j.cub.2013.09.013.

Acknowledgments

We thank Kor Brandsma for assistance with surgical procedures and animal training. This work was supported by an NWO-VICI grant, an HFSP grant, support from the European Union Seventh Framework Programme (project 269921 "BrainScaleS") awarded to P.R.R., and an NWO-VIDI grant awarded to H.S.

Received: May 19, 2013
Revised: August 14, 2013
Accepted: September 4, 2013
Published: October 17, 2013

References

1. Douglas, R.J., and Martin, K.A. (2004). Neuronal circuits of the neocortex. Annu. Rev. Neurosci. *27*, 419–451.
2. Callaway, E.M. (1998). Local circuits in primary visual cortex of the macaque monkey. Annu. Rev. Neurosci. *21*, 47–74.
3. Lund, J.S. (1988). Anatomical organization of macaque monkey striate visual cortex. Annu. Rev. Neurosci. *11*, 253–288.
4. Henry, G.H., Harvey, A.R., and Lund, J.S. (1979). The afferent connections and laminar distribution of cells in the cat striate cortex. J. Comp. Neurol. *187*, 725–744.
5. Larkum, M. (2013). A cellular mechanism for cortical associations: an organizing principle for the cerebral cortex. Trends Neurosci. *36*, 141–151.
6. Blasdel, G.G., and Lund, J.S. (1983). Termination of afferent axons in macaque striate cortex. J. Neurosci. *3*, 1389–1413.
7. Hubel, D.H., and Wiesel, T.N. (1972). Laminar and columnar distribution of geniculo-cortical fibers in the macaque monkey. J. Comp. Neurol. *146*, 421–450.
8. Gilbert, C.D., and Wiesel, T.N. (1983). Clustered intrinsic connections in cat visual cortex. J. Neurosci. *3*, 1116–1133.
9. Rockland, K.S., and Pandya, D.N. (1979). Laminar origins and terminations of cortical connections of the occipital lobe in the rhesus monkey. Brain Res. *179*, 3–20.
10. Rockland, K.S., and Virga, A. (1989). Terminal arbors of individual "feedback" axons projecting from area V2 to V1 in the macaque monkey: a study using immunohistochemistry of anterogradely transported Phaseolus vulgaris-leucoagglutinin. J. Comp. Neurol. *285*, 54–72.
11. Anderson, J.C., and Martin, K.A. (2009). The synaptic connections between cortical areas V1 and V2 in macaque monkey. J. Neurosci. *29*, 11283–11293.
12. Felleman, D.J., and Van Essen, D.C. (1991). Distributed hierarchical processing in the primate cerebral cortex. Cereb. Cortex *1*, 1–47.
13. Lamme, V.A., and Roelfsema, P.R. (2000). The distinct modes of vision offered by feedforward and recurrent processing. Trends Neurosci. *23*, 571–579.
14. Mumford, D., Kosslyn, S.M., Hillger, L.A., and Herrnstein, R.J. (1987). Discriminating figure from ground: the role of edge detection and region growing. Proc. Natl. Acad. Sci. USA *84*, 7354–7358.
15. Wolfson, S.S., and Landy, M.S. (1998). Examining edge- and region-based texture analysis mechanisms. Vision Res. *38*, 439–446.
16. Roelfsema, P.R., Lamme, V.A., Spekreijse, H., and Bosch, H. (2002). Figure-ground segregation in a recurrent network architecture. J. Cogn. Neurosci. *14*, 525–537.
17. Grossberg, S., and Mingolla, E. (1985). Neural dynamics of form perception: boundary completion, illusory figures, and neon color spreading. Psychol. Rev. *92*, 173–211.
18. Poort, J., Raudies, F., Wannig, A., Lamme, V.A., Neumann, H., and Roelfsema, P.R. (2012). The role of attention in figure-ground segregation in areas V1 and V4 of the visual cortex. Neuron *75*, 143–156.
19. Ferster, D., and Miller, K.D. (2000). Neural mechanisms of orientation selectivity in the visual cortex. Annu. Rev. Neurosci. *23*, 441–471.
20. Bhatt, R., Carpenter, G.A., and Grossberg, S. (2007). Texture segregation by visual cortex: perceptual grouping, attention, and learning. Vision Res. *47*, 3173–3211.
21. Li, Z. (1999). Visual segmentation by contextual influences via intracortical interactions in the primary visual cortex. Network *10*, 187–212.
22. Lamme, V.A. (1995). The neurophysiology of figure-ground segregation in primary visual cortex. J. Neurosci. *15*, 1605–1615.
23. Supèr, H., Spekreijse, H., and Lamme, V.A. (2001). Two distinct modes of sensory processing observed in monkey primary visual cortex (V1). Nat. Neurosci. *4*, 304–310.
24. Lamme, V.A., Zipser, K., and Spekreijse, H. (1998). Figure-ground activity in primary visual cortex is suppressed by anesthesia. Proc. Natl. Acad. Sci. USA *95*, 3263–3268.
25. Mitzdorf, U. (1985). Current source-density method and application in cat cerebral cortex: investigation of evoked potentials and EEG phenomena. Physiol. Rev. *65*, 37–100.

26. Lund, J.S. (1973). Organization of neurons in the visual cortex, area 17, of the monkey (Macaca mulatta). J. Comp. Neurol. *147*, 455–496.
27. Maunsell, J.H., and Gibson, J.R. (1992). Visual response latencies in striate cortex of the macaque monkey. J. Neurophysiol. *68*, 1332–1344.
28. Nowak, L.G., Munk, M.H., Girard, P., and Bullier, J. (1995). Visual latencies in areas V1 and V2 of the macaque monkey. Vis. Neurosci. *12*, 371–384.
29. Gilbert, C.D. (1983). Microcircuitry of the visual cortex. Annu. Rev. Neurosci. *6*, 217–247.
30. Katz, L.C., Gilbert, C.D., and Wiesel, T.N. (1989). Local circuits and ocular dominance columns in monkey striate cortex. J. Neurosci. *9*, 1389–1399.
31. Binzegger, T., Douglas, R.J., and Martin, K.A. (2004). A quantitative map of the circuit of cat primary visual cortex. J. Neurosci. *24*, 8441–8453.
32. Larkum, M.E., Senn, W., and Lüscher, H.R. (2004). Top-down dendritic input increases the gain of layer 5 pyramidal neurons. Cereb. Cortex *14*, 1059–1070.
33. Maier, A., Aura, C.J., and Leopold, D.A. (2011). Infragranular sources of sustained local field potential responses in macaque primary visual cortex. J. Neurosci. *31*, 1971–1980.
34. Xing, D., Yeh, C.I., Burns, S., and Shapley, R.M. (2012). Laminar analysis of visually evoked activity in the primary visual cortex. Proc. Natl. Acad. Sci. USA *109*, 13871–13876.
35. Nothdurft, H.C., Gallant, J.L., and Van Essen, D.C. (2000). Response profiles to texture border patterns in area V1. Vis. Neurosci. *17*, 421–436.
36. Knierim, J.J., and van Essen, D.C. (1992). Neuronal responses to static texture patterns in area V1 of the alert macaque monkey. J. Neurophysiol. *67*, 961–980.
37. Nothdurft, H.C., Gallant, J.L., and Van Essen, D.C. (1999). Response modulation by texture surround in primate area V1: correlates of "pop-out" under anesthesia. Vis. Neurosci. *16*, 15–34.
38. Henry, C.A., Joshi, S., Xing, D., Shapley, R.M., and Hawken, M.J. (2013). Functional characterization of the extraclassical receptive field in macaque V1: contrast, orientation, and temporal dynamics. J. Neurosci. *33*, 6230–6242.
39. Lamme, V.A., Rodriguez-Rodriguez, V., and Spekreijse, H. (1999). Separate processing dynamics for texture elements, boundaries and surfaces in primary visual cortex of the macaque monkey. Cereb. Cortex *9*, 406–413.
40. Hirsch, J.A., and Gilbert, C.D. (1991). Synaptic physiology of horizontal connections in the cat's visual cortex. J. Neurosci. *11*, 1800–1809.
41. Gilbert, C.D., and Wiesel, T.N. (1979). Morphology and intracortical projections of functionally characterised neurones in the cat visual cortex. Nature *280*, 120–125.
42. Malach, R., Amir, Y., Harel, M., and Grinvald, A. (1993). Relationship between intrinsic connections and functional architecture revealed by optical imaging and in vivo targeted biocytin injections in primate striate cortex. Proc. Natl. Acad. Sci. USA *90*, 10469–10473.
43. Hupé, J.M., James, A.C., Girard, P., and Bullier, J. (2001). Response modulations by static texture surround in area V1 of the macaque monkey do not depend on feedback connections from V2. J. Neurophysiol. *85*, 146–163.
44. Craft, E., Schütze, H., Niebur, E., and von der Heydt, R. (2007). A neural model of figure-ground organization. J. Neurophysiol. *97*, 4310–4326.
45. Lamme, V.A., Supèr, H., and Spekreijse, H. (1998). Feedforward, horizontal, and feedback processing in the visual cortex. Curr. Opin. Neurobiol. *8*, 529–535.
46. Rockland, K.S., Saleem, K.S., and Tanaka, K. (1994). Divergent feedback connections from areas V4 and TEO in the macaque. Vis. Neurosci. *11*, 579–600.
47. Rockland, K.S., and Knutson, T. (2000). Feedback connections from area MT of the squirrel monkey to areas V1 and V2. J. Comp. Neurol. *425*, 345–368.
48. Moore, T., and Armstrong, K.M. (2003). Selective gating of visual signals by microstimulation of frontal cortex. Nature *421*, 370–373.
49. Ekstrom, L.B., Roelfsema, P.R., Arsenault, J.T., Bonmassar, G., and Vanduffel, W. (2008). Bottom-up dependent gating of frontal signals in early visual cortex. Science *321*, 414–417.
50. Self, M.W., Kooijmans, R.N., Supèr, H., Lamme, V.A., and Roelfsema, P.R. (2012). Different glutamate receptors convey feedforward and recurrent processing in macaque V1. Proc. Natl. Acad. Sci. USA *109*, 11031–11036.